

# USE OF LIDAR AND RADAR DATA FOR CIRRUS CLOUD MODEL INITIALIZATION AND VALIDATION

Jennifer M. Comstock<sup>(1)</sup>, Ruei-Fong Lin<sup>(2,3)</sup>, David O. Starr<sup>(2)</sup>, and Sally A. McFarlane<sup>(1)</sup>

(1) Pacific Northwest National Laboratory, Richland, WA, USA

(2) NASA-Goddard Space Flight Center, Greenbelt MD, USA

(3) University of Maryland, Baltimore County, Baltimore MD, USA

## ABSTRACT

Cirrus formation processes and their relationship to cloud microphysical properties have important implications for cloud-radiative feedback and climate model studies. We use Raman lidar water vapor measurements to initialize a 1-dimensional (1D) cirrus model with explicit microphysics to simulate cloud microphysical properties and the particle size distribution. In addition, we compare model output with Raman lidar extinction and radar reflectivity measurements, and with combined radar-lidar retrievals of cirrus microphysical properties. The main focus of this study is to understand how well the 1D model can simulate observed cloud properties, which will allow us to use this approach for analysis of cloud formation processes and for parameterization development.

## 1. MEASUREMENTS AND MICROPHYSICS RETRIEVAL ALGORITHM

The United States Department of Energy, Atmospheric Radiation Measurement (ARM) program operates a Raman Lidar (RL) and Millimeter Cloud Radar (MMCR) at the Southern Great Plains (SGP) Climate Research Facility (CRF) located at 36° 37' N, 97° 30' W. In addition to these active remote sensors, the ARM SGP site includes a wide array of solar, infrared, and microwave radiometers, four times daily radiosonde launches and surface and tower meteorological measurements (see [www.arm.gov](http://www.arm.gov) for more details).

The ARM RL [1] is a continuously operating, automated lidar that transmits a laser pulse at 355 nm, which undergoes elastic scattering due to clouds and aerosols. The ARM RL also detects inelastic scattered photons produced by the rotational-vibrational Raman effect of nitrogen (387 nm) and water vapor (408 nm) molecules. The water vapor mixing ratio ( $q$ ) is proportional to the ratio of the water vapor and nitrogen signals, which are measured simultaneously. The RL  $q$  data are calibrated to agree with co-located microwave radiometer column water vapor measurements [2]. The RL provides  $q$  profiles at 10 min intervals with an accuracy of ~5% [3], and have been used to analyze ice supersaturation in cirrus clouds [4]. In addition to water vapor, we retrieve profiles of the extinction coefficient ( $\beta_e$ ) at 387 nm by calculating the slope of the nitrogen signal [5].

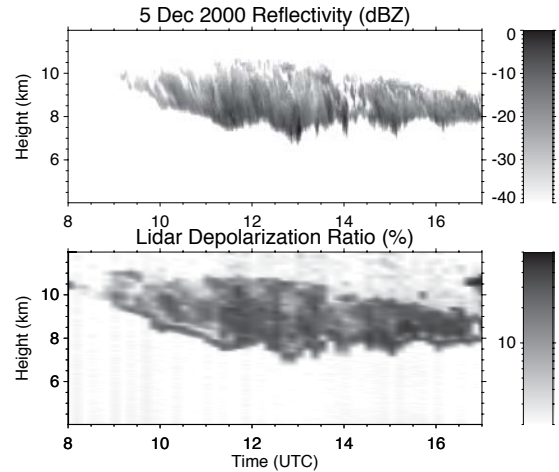


Fig. 1. Height vs. time display of radar reflectivity (top) and Raman lidar depolarization ratio (bottom) observed on 5 December 2000 at the ARM SGP CRF.

The ARM MMCR also operates continuously at 35 GHz and measures reflectivity, Doppler velocity, and spectral width. More recently, the MMCR has been upgraded to record full Doppler spectra. The reflectivity measurement has an uncertainty of ~0.5 dB and a minimum detectable signal of ~-47 dB at 10 km. Figure 1 depicts the RL depolarization ratio and MMCR reflectivity measurements observed on 5 December 2000 at the ARM SGP site. Since upper tropospheric water vapor measurements are only available when the signal-to-noise ratio is reasonable, we limit the study to nighttime observations.

The ARM SGP site also houses an eye safe Micropulse Lidar (MPL) [6], which operates at 523 nm with a pulse repetition frequency (PRF) of 2500 Hz, maximum output energy of 10-15  $\mu$ J, and a 100  $\mu$ rad receiver field-of-view. The recorded resolution is 30 m vertically and 60 sec temporally.

We combine the MMCR reflectivity and MPL backscatter measurements to retrieve the effective particle size ( $r_{\text{eff}}$ ) and ice water content (IWC) following the algorithm of Donovan and van Lammeren [7]. The lidar-radar algorithm is a robust algorithm that utilizes the ratio of the sixth moment to the second moment of the particle size distribution (PSD) to retrieve  $r_{\text{eff}}$ . This arises from the fact that lidar wavelengths are sensitive

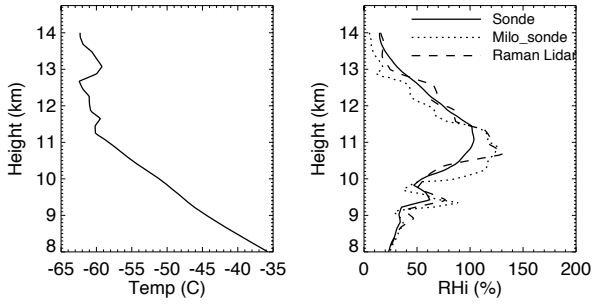


Fig. 2. Profiles of temperature (left) and RHI (right) used to initialize the 1D model.

to smaller particles ( $r^2$ ), whereas the radar wavelengths are sensitive larger particles ( $r^6$ ). We have modified the Donovan and van Lammeren algorithm to account for different particle shapes. Retrieved microphysical properties from this algorithm compare reasonably well with field observations [8] and have been used to compare cloud properties at European CloudNET and ARM sites [9].

## 2. CIRRUS CLOUD MODEL

We use a 1-dimensional (1D) cloud model with an explicit microphysical scheme that treats both heterogeneous and homogeneous nucleation, to simulate cirrus clouds observed over the ARM SGP site. Both ice crystals and  $H_2SO_4$  aerosol particles are binned according to mass, allowing us to reconstruct the particle size distribution at each atmospheric level. The model also includes diffusional growth, aggregation, and vertical transport of ice crystals. Recently, the model has been upgraded to include direct radiative effects on ice crystals, horizontal advection of water vapor and dry static energy, and a variable vertical velocity profile. Further model details are available in Lin et al. [10].

## 3. MODEL INITIALIZATION WITH LIDAR WATER VAPOR PROFILES

Model initialization requires profiles of pressure, temperature and  $q$ , from which the relative humidity with respect to ice (RHI) can be calculated. Initiation of ice crystal formation is closely linked with RHI. Heterogeneous nucleation typically occurs under conditions of small RHI ( $<120\%$ ), whereas homogeneous nucleation requires large RHI ( $>150\%$ ). We compare the effects of changes in the water vapor profile on the simulated microphysical properties and compare the model output with radar and lidar observations. Figure 2 depicts the profiles of RHI for three model runs. The control run is labeled “Sonde” and denotes the  $q$  profile measured by a Vaisala RS-80 radiosonde. The run labeled as “Milo-sonde” denotes the same radiosonde  $q$  profile, but with corrections made for the dry bias that occurs at cold temperatures using the Miloshevich et al. technique [11]. Note that all

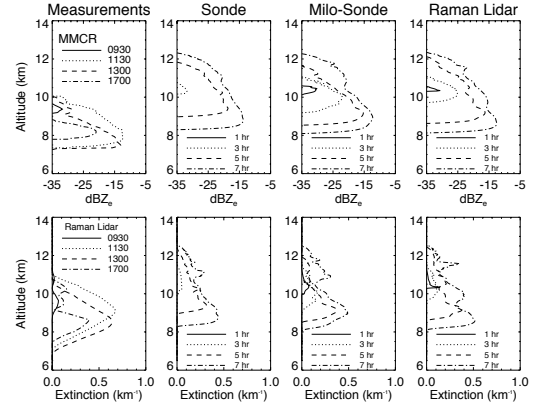


Fig. 3. Comparison of measured radar reflectivity and Raman lidar extinction coefficient with simulated profiles. Measured profiles are averaged for 6 minutes temporally.

model simulations assume that the ice crystal shape is columns.

## 4. COMPARISONS WITH RADAR REFLECTIVITY AND LIDAR EXTINCTION MEASUREMENTS

Since the 1D model simulates the particle size distribution, we can calculate the equivalent radar reflectivity ( $Z_e$ ) and extinction coefficient ( $\beta_e$ ) at the lidar wavelength. One benefit of this approach is that the uncertainty of comparing with retrieved microphysical properties (such as IWC or  $r_{eff}$ ) is eliminated. For the  $\beta_e$  calculations, we assume columnar shaped particles and use the scattering properties from Yang et al. [12]. Comparisons of  $Z_e$  (Fig. 3) reveal that the maximum simulated  $Z_e$  for all model runs compares well with measurements. The simulated  $\beta_e$  also compare well with observations, with the “Sonde” run having slightly smaller peak values.

It is noticeable in Fig. 3 that the simulated cloud morphology or evolution does not compare well with observations. For example, the cloud depth is similar, but the location of the cloud is not. These differences may be due to the idealized nature of the 1D model and the simplified dynamics, which neglect horizontal transport of condensate and small scale turbulence. The vertical structure of the simulated  $\beta_e$  shows slightly larger values than observed near cloud top. It is also notable that the lidar detects ice crystals at a higher altitude than the radar, implying the presence of small crystals near cloud top. In contrast, the simulated  $Z_e$  is large near the cloud top. This occurs because the simulated PSD predicts ice crystals that are too large near cloud top (crystals grow too quickly).

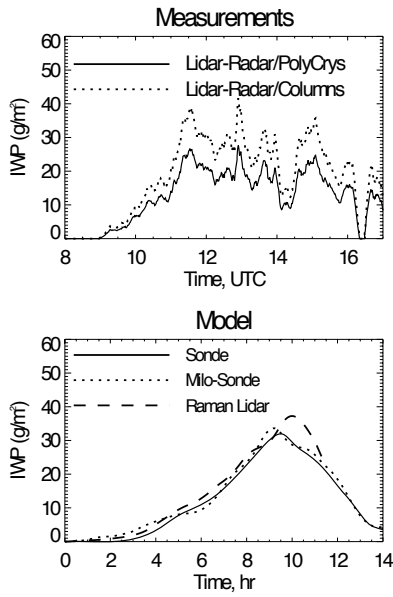


Fig. 4. Comparison of lidar-radar retrieved IWP (top) and modeled values (bottom).

## 5. COMPARISONS OF MICROPHYSICAL PROPERTIES

We also compare the evolution of simulated mean layer microphysical properties with those retrieved using the Donovan and van Lammeren algorithm. Retrieved quantities are shown for two different ice crystal shapes. Due to the simplified dynamics in the 1D model, we do not expect to simulate the small scale fluctuations in the microphysical properties, but are attempting to simulate the gross characteristics of the cloud.

Comparisons of ice water path (IWP) (Fig. 4) reveals that the maximum modeled IWP using the sonde data is  $\sim 35 \text{ g m}^{-2}$  whereas the retrieved values vary between 20 and  $40 \text{ g m}^{-2}$  depending on the assumed crystal shape. The model run using the RL water vapor profile has slightly larger IWP than the sonde runs, reaching a maximum of nearly  $40 \text{ g m}^{-2}$ . Note that the simulation time ( $\sim 14 \text{ hr}$ ) does not match well with the measured cloud time period. In Figs. 4-6, we plot only  $\sim 9 \text{ hrs}$  of the measured cloud evolution because a second cloud layer forms above the cloud of interest. The discrepancy between the modeled and measured temporal scales is due to small scale advection of  $q$ . Horizontal advection of condensate is minimal for this case.

Next we compare the  $r_{\text{eff}}$  derived from model simulations and measurements (Fig. 5). The retrieved  $r_{\text{eff}}$  varies between  $\sim 20$  and  $40 \mu\text{m}$  depending on crystal shape, and is larger for columns. The  $r_{\text{eff}}$  does not vary significantly between the three model runs, except in the first 4 hr of the simulation with a maximum value

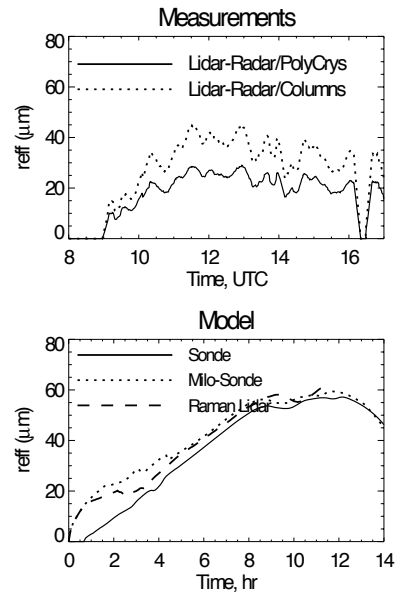


Fig. 5. As in Fig. 4 but for  $r_{\text{eff}}$ .

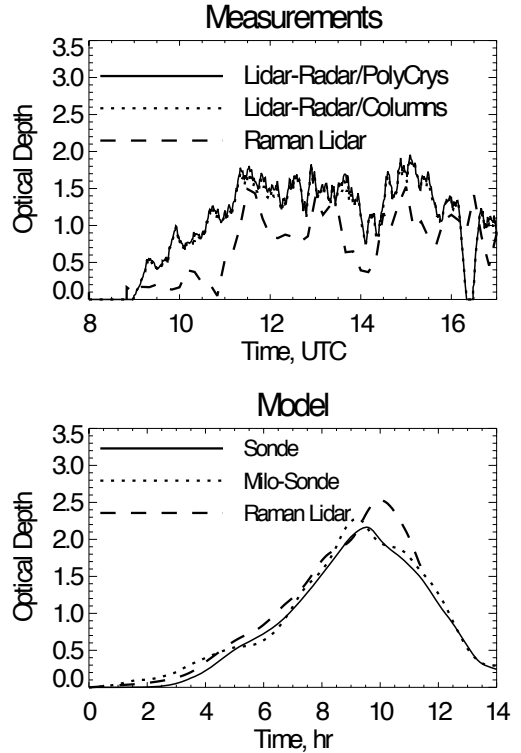


Fig. 6. As in Fig. 4 but for optical depth.

approaching  $60 \mu\text{m}$ . The simulated  $r_{\text{eff}}$  is generally larger than the measured values.

Finally, we compare the evolution of the optical depth ( $\tau$ ; Fig. 6). In addition to the lidar-radar retrieved  $\tau$ , we also include  $\tau$  derived from the Raman Lidar backscatter profiles using a Beer's Law approach. The RL measured  $\tau$  is noticeably smaller than the lidar-radar retrieved values. Due to the nature of the retrieval,  $\tau$  does not vary with crystal habit. The simulated  $\tau$  using the sonde

profiles have a maximum value of  $\sim 2.0$ , which compares well with the lidar-radar retrieved  $\tau$ . The simulated  $\tau$  using the RL  $q$  profile is slightly larger than the other model runs.

## 6. DISCUSSION AND SUMMARY

In this study, we utilize the ground based active remote sensors at the ARM SGP site for initialization and validation of a 1D cirrus cloud model with explicit binned microphysics. We have shown that model runs initialized with Raman lidar  $q$  profiles compare well with runs using radiosonde  $q$  profiles, particularly when the sonde profiles are corrected for dry bias. This result gives us confidence in using RL  $q$  profiles between radiosonde launch times. Although the cloud position is slightly higher than the measurements, the cloud depth is similar.

Model values of  $Z_e$  and  $\beta_e$  compare well with observations, which implies that the PSD is reasonable. However, near cloud top, there appears to be too many large particles. Note that the simulated PSD (not shown) exhibits a bimodal shape in the top third of the cloud (below the nucleation zone), a narrow mono-modal distribution mid-cloud, and a broad gamma distribution weighted toward large particles near cloud base.

Comparisons between model and retrieved microphysical properties reveals that small scale fluctuations in the observed cloud are not simulated well, but the maximum values are reasonable, particularly for IWP and  $\tau$ . The underestimation of IWP and  $\tau$  in the first few hours of the simulation appears to be caused by too few small particles. Modeled  $r_{\text{eff}}$  are generally larger than retrieved values.

These comparisons suggest that the 1D model driven by the RL  $q$  profiles combined with observations provides a useful framework for understanding the physical processes that determine the microphysical properties in cirrus clouds. Future comparisons with *in situ* measurements will help to validate the simulated PSD. To help improve simulations, we plan to examine the use of satellite imagery to account for horizontal advection of condensate, and the use of radar Doppler velocity measurements to investigate the fall velocity of ice crystals.

## 7. ACKNOWLEDGEMENTS

This research is funded by the U.S. Department of Energy, Office of Science, Atmospheric Radiation Measurement Program. We thank D. Donovan and G.-J. van Zadelhoff for supplying the lidar-radar retrieval code. We also thank L. Miloshevich and D. Turner for supplying the corrected radiosonde data.

## 8. REFERENCES

1. Goldsmith, J. E. M., F. H. Blair, S. E. Bisson, and D. D. Turner (1998), *Appl. Opt.*, 37, 4979-4990.

2. Turner, D. D., and J. E. M. Goldsmith (1999), Twenty-four-hour Raman lidar water vapor measurements during the Atmospheric Radiation Measurement program's 1996 and 1997 water vapor intensive observation periods, *J. Atmos. Ocean. Tech.*, 16, 1062-1076.

3. Ferrare, R. A., and coauthors (2004), Characterization of upper tropospheric water vapor measurements during AFWEX using LASE. *J. of Atmos. Ocean. Tech.*, in press.

4. Comstock, J. M., T. P. Ackerman, and D. D. Turner (2004), Evidence of high ice supersaturation in cirrus clouds using ARM Raman lidar measurements. *Geophys. Res. Lett.*, doi:10.1029/2004GL019705.

5. Ansmann, A., U. Wandinger, M. Riebesell, C. Weitkamp, and W. Michaelis, 1992: Independent measurement of extinction and backscatter profiles in cirrus clouds by using a combined Raman elastic-backscatter lidar. *Appl. Opt.*, 31, 7113-7131.

6. Campbell, J. R., and coauthors, 2002: Full-time, eye-safe cloud and aerosol lidar observation at atmospheric radiation measurement program sites: instruments and data processing. *J. Atmos. Oce. Technol.*, 19, 431-442.

7. Donovan, D. P., and A. C. A. P. van Lammeren, 2001: Cloud effective particle size and water content profile retrievals using combined lidar and radar observations 1. Theory and examples. *J. Geophys. Res.*, 106, 27425-27448.

8. Donovan, D. P., and coauthors (2001): Cloud effective particle size and water content profile retrievals using combined lidar and radar observations 2. Comparison with IR radiometer and in situ measurements of ice clouds. *J. Geophys. Res.*, 106, 27449-27464.

9. van Zadelhoff, G. J., D. P. Donovan, H. K. Baltink, and (2004), Comparing ice cloud microphysical properties using CloudNET and atmospheric radiation measurement program data. *J. Geophys. Res.*, 109,

10. Lin, R.-F., D. O'C. Starr, J. Reichardt, and P. J. DeMott, 2005: Nucleation in synoptically forced cirrostratus. *J. Geophys. Res.*, 110, doi10.1029/2004JD005362.

11. Miloshevich, L. M., H. Vomel, A. Paukkunen, A. J. Heymsfield, S. J. Oltmans, 2001: Characterization and correction of relative humidity measurements from Vaisala RS80-A radiosondes at cold temperatures. *J. Atmos. Ocean. Tech.*, 18, 135-156.

12. Yang, P., K.N. Liou, K. Wyser, and D. Mitchell, 2000: Parameterization of the scattering and absorption properties of individual ice crystals. *J. Geophys. Res.*, 105, 4699-4718.